International Journal of Science and Research (IJSR)
ISSN (Online): 2319-7064
Index Copernicus Value (2013): 6.14 | Impact Factor (2015): 6.391

Modeling Infrared (IR) Emission of Novae

Suliman Mohamed Osman

Physics Department, Faculty of Science, Albaha University, Albaha, Saudi Arabia

Abstract: ***IR emission of dusty classical novae is modeled for a blob- ring shell geometry having carbon (graphite) grains in the blobs and silicate grains in the ring. Specific characteristics of the temporal and wavelength dependence of the theoretical IR fluxes from the model are predicted and compared with observations of some classical novae. The theoretical calculations of the model show general agreement with observations.***

Keywords: Model, Infrared emission, Novae, observation, Dust formation, Light curves

1. Introduction

The idea of the presence of dust shells around novae has been known for long time. However, to detect a shell of dust we must look for IR excess. IR excess is defined as, excess emission at infrared wavelengths over what we would expect to receive from the photosphere of the star alone. In other words, dust grains effectively remove some of the short wavelength energy flux from the star and re-emit it at longer (infrared) wavelengths.

Besides, observations at infrared wavelengths, optical region can provide a wealth of information about the grains and can give a rough estimate for the temperature of the nova as well. For example, the optical light curves can give a clue to the existence of a dust shell. So to look for observational proof for dust shells around novae optical, ultraviolet and infrared observations of specific nova should be examined.

2. Observations

2.1 Optical Observations

The ideal light curve with three possible behavior during the transition phase is that given in (Fig. 1) [13]. From the figure the behavior of the nova during transition phase can be divided into three types:

- Novae which pass into a deep minimum, 7-8 magnitude deep. And lasting for 2-3 months, after which the star brightens to follow its late decline (e.g. DQ Her 1934) (Fig. 2). This is the case we are studying now.
- Novae which go into large oscillations (1.2 magnitudes) as they pass through the transition phase (e.g. V603 Aql.)
- Novae which pass the transition phase without noticeable peculiarity in their light curves.

The break in the optical decline of the light curves during the transition phase, in general is attributed to the formation of dust shell out of the expanding eject a as a result of cooling processes.

2.2 Infrared Observations

Extensive coverage of NQ Vul provided the first complete record of formation of an optically thick dust shell [17]. Observation for Nova Aquilae 1982, has shown the infrared emission and visual light curve for the nova (Fig. 4). Spectrometry for the same nova in the range 2-4 μm was obtained (Fig. 5). (Fig. 6) shows the optical and infrared light curves of Nova Centauri 1986. From the figure one can easily notice coincidence of optical light curve drop with the excess of the infrared emission. Recent Observation data in optical and near-infrared of several Novae is available in [4] .

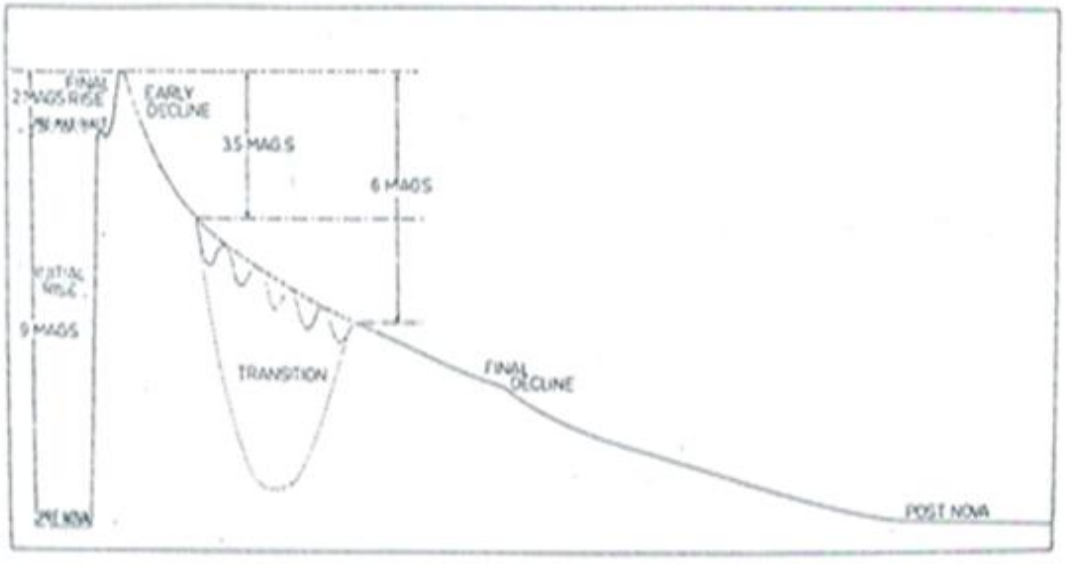

Fig 1: Morphology of a nova light curve. From Mclaughlin (1960).

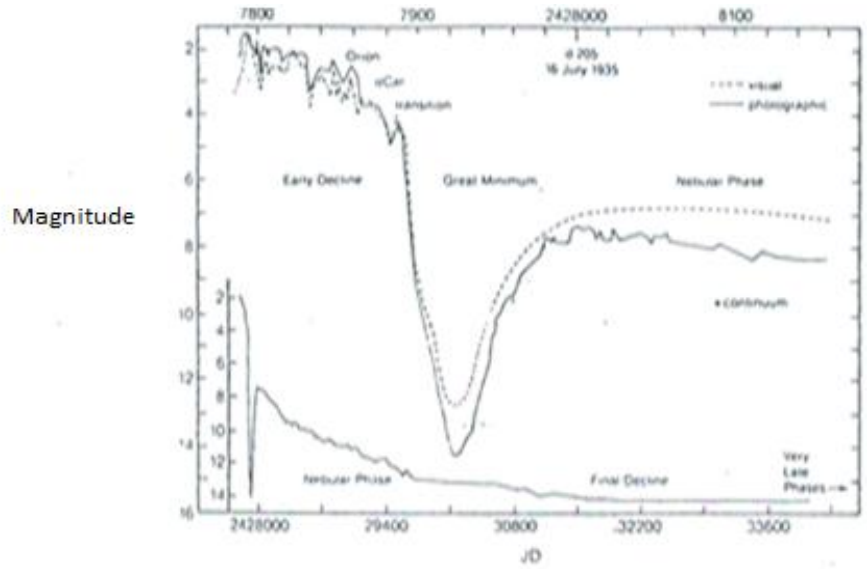

Fig. 2 : Light curves for Nova DQ Her 1934, identifying the main phases in the evolution. The magnitudes include continuum plus line contributions to the light. The visual data is taken from Mattei (1984), whereas the extensive photographic coverage is by Gaposchkin (1956).

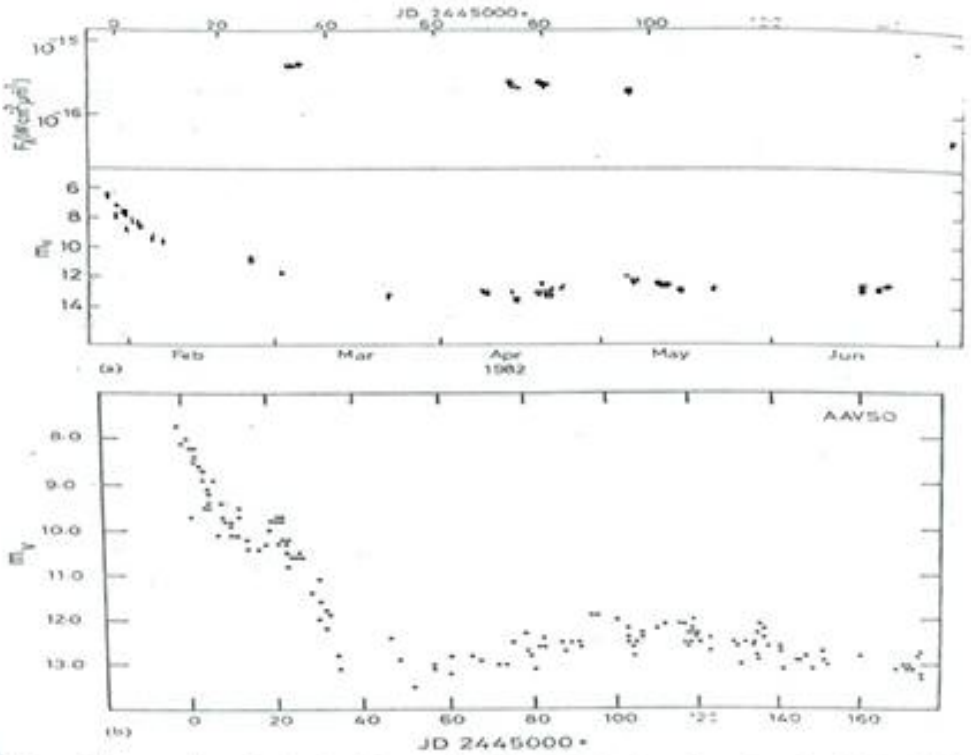

Fig. 4 : Observation data for Nova Aquilae 1982. (a; above) The 'Visual' light curve (bottom) is a heterogeneous mix of visual estimates (·), IUE FES (+), and V band photometric (◎) observations. The infrared light curve (top) is from K band photometry where the most complete set of data exists. (b; below) visual light curve from AAVSO observations. From Bode et al. (1984).

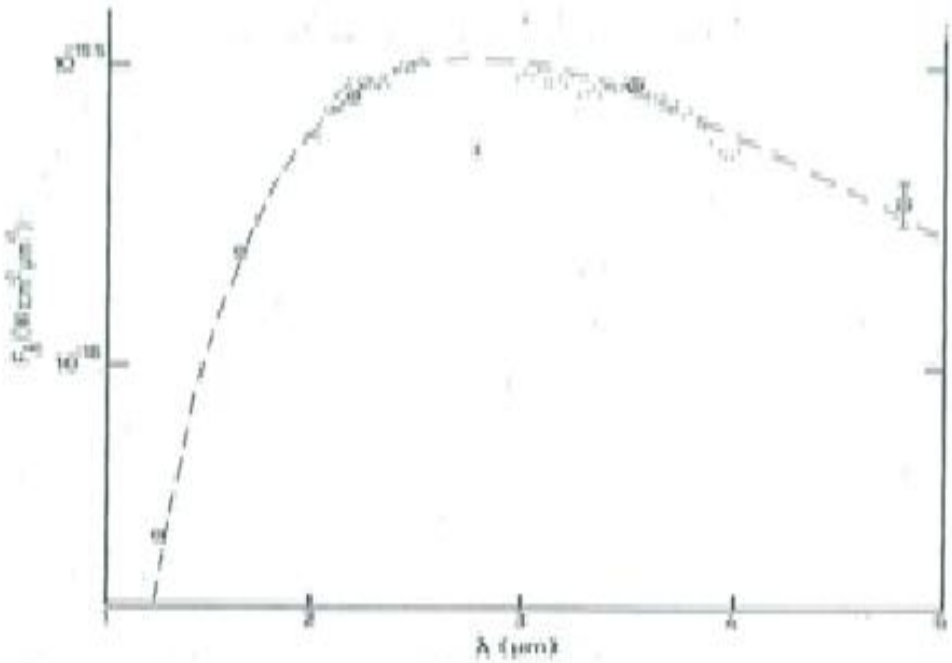

Fig. 5: The smoothed 1982 April 18.1 CVF spectrum and J, H, K, L, and M photometry for Nova Aquilae 1982. The fitted 1010 K blackbody curve is superimposed. A typical error bar for the CVF data is shown. From Bode et al. (1984).

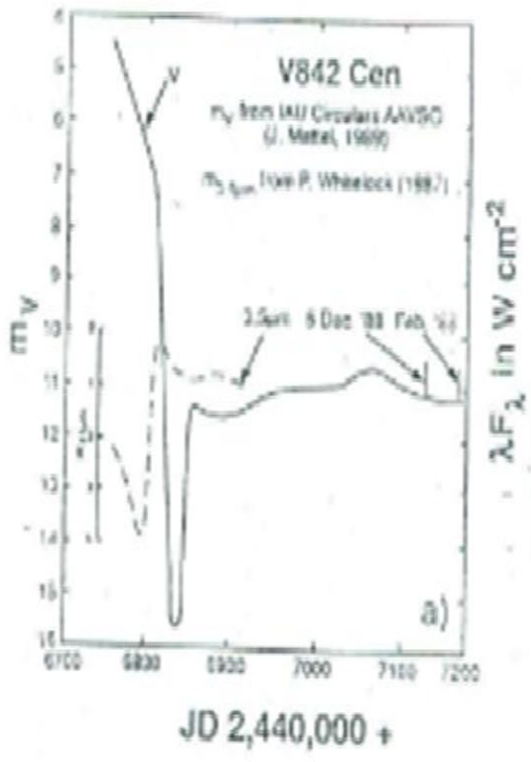

Fig. 6: Optical and Infrared Light curves of Nova Centauri 1986. Taken from Gehrz (1990).

3. Classical Novae and Dust shell

3.1 Classical Novae Theory

Classical novae are known as binary system which undergoes dramatic unpredictable increases in apparent luminosity which may rival the apparent luminosity of the brightest starts in the sky (e.g. Sirius). The high increase in nova luminosity is proven to be due to thermonuclear runaway (TNR) given the correct conditions. In the explosion part of the mass of the nova is ejected, which moves outward and start to cool gradually forming a shell of grains around the nova.

The idea of non-homogeneous envelope (shell) around novae has been made since the time of nova Aquilae 1918 (v603 Aql). Later Mustel et al. (1970) put forward the argument that the envelopes of all such objects (e.g. nova Aquilae 1918, nova HR Delphini1967, nova Volpecule 1968, nova Serpentis 1970 and nova Cygni (1975, 1978) have a characteristic spatial structure with material concentrated in the polar caps (or blobs) and in equatorial belts (or ring) [15]. These suggestions are also inferred from the analysis of direct photographs (Fig. 7). Also observations in infrared and optical region of X-ray transient object CI Cam has shown non spherical shell [16].

The theoretical work of Hutching (1972) supported non-spherical structure at least for three novae (i.e. nova Delphini 1967, nova vulpecule 1968 and nova Serpentis 1970) [11]. Additional evidence for non-spherical structure comes from the CCD images of some novae [5]. Also the narrow-band CCD images of nova HR Delphini (1967) [10], [18]. show an oval shape of the remnant possessing a bipolar morphology, with polar 'blobs' and, an equatorial ring – like structure. Our model will assume a blob-ring structure (Fig. 8) for the IR emission calculations.

3.2 Dust Formation (Grains)

After a nova eruption, a mass of $10^{-5} - 10^{-4}\ M$ is ejected, which moves outwards and start to coal and condense (Temp.

decreases) forming dust grains with size as a function of time given by the following equation:

$$a = a_0 + a_\infty[1 - (\frac{t}{t_0})^{-\frac{5}{4}}] \quad (1)$$

a_0 : radius of condensation nucleus, taken to be 10^{-7}cm [20]. a_∞ :maximum radius ≈ 0.15 μm ≈1.5x10^{-5} cm.

The ratio of C/O observed to reverse in the ejecta of some novae (e.g. Qv vul 1987) leading to the formation of two or more types of grains in the same ejecta [7], [1]. For the interest of this work, grains of carbon (graphite) and silicates will be considered to co-exist in our model. Graphite in the blobs and silicates in the equatorial ring.

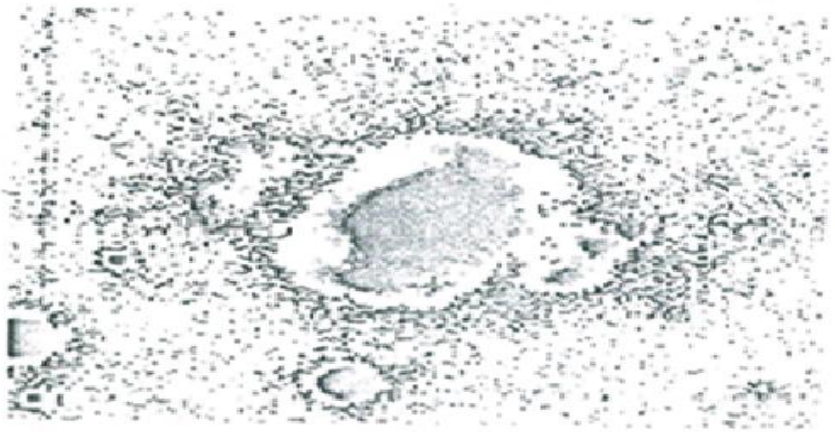

Figure 7: The photograph of the ring and two blobs shells surrounding Nova RR Pic 1925 taken through an H_α filter. From Duerbeck (1987)

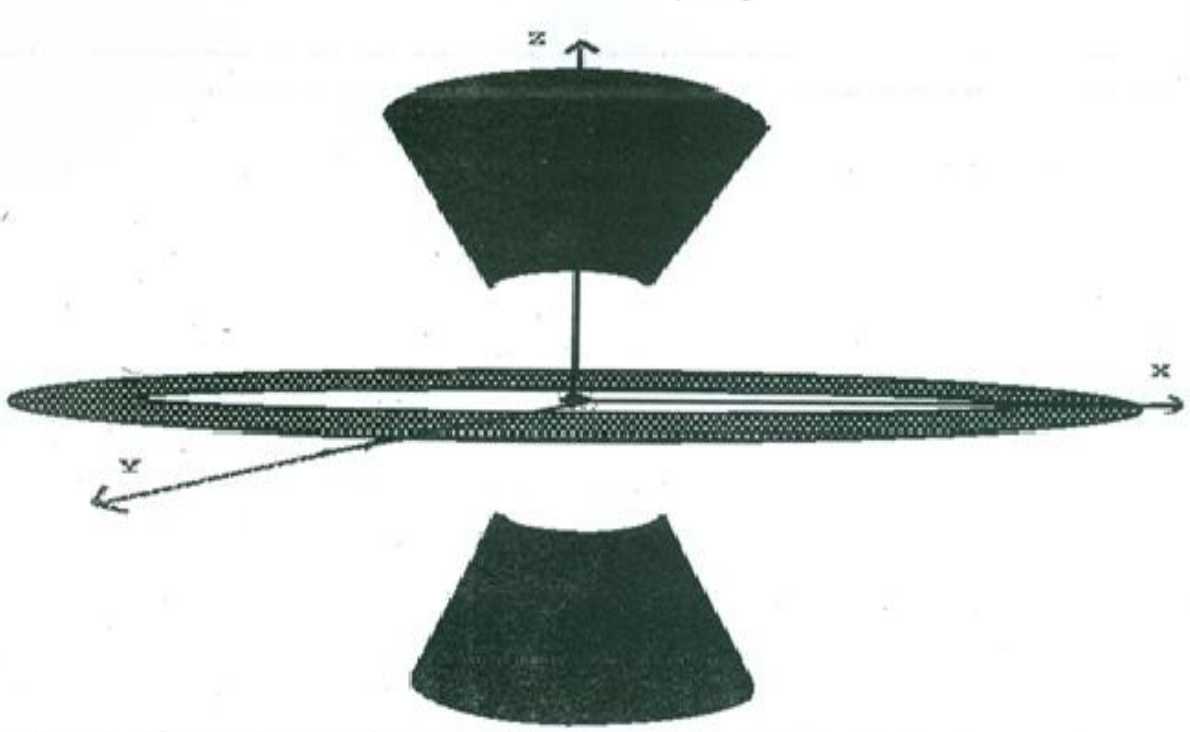

Figure 8: Schematic diagram of the blob/ring geometry assumed for the theoretical calculations.

4. IR Emission Formulae

This section will state the IR flux calculations formulae for the blobs-ring model having graphite in the blobs and silicates in the ring. The calculated IR fluxes of the model will be compared with observed IR light curves and energy distributions of some novae (already discussed in IR observation section).

4.1 The Model Formulae

For spherical optically thin dust shell the emitted intensity (equation of transfer; (see Evans, 1993) is:

$$I_\nu(s) = I_\nu(0)e^{-\tau(s,0)} + \int_0^{\tau(s)} e^{-\tau(s,\acute{s})} S_\nu d\tau \quad (2)$$

The first term is the intensity of radiation at the far side of the source I_ν, attenuated by a factor $e^{-\tau(s,0)}$ by extinction within the medium.

The second term represents emission from within the medium at ś attenuated by the appropriate factor and integrated along the line of sight between 0 and s. In our case only this term is important, since the emission from the first term will have negligible effect at IR wavelengths. The source function S_ν can be replaced by the Planck function B(ν, T_g) for purely thermal radiation and with the use of $d\tau = N\pi a^2 Q_{abs}\, ds$ then

$$I_\nu(s) = \int_0^s B\left(\nu, T_g(\nu)\right) e^{-\tau(\nu)}\, N(r)\pi a^2 Q_{abs}\, ds \quad (3)$$

Where ν is the frequency, T_g is the grain temperature, N(r) is the dust number density at distance r from the central star, a is the grain radius and Q_{abs} is the absorption efficiency. Equation (3) can be expressed as:

$$I_\nu(s) = \int_0^s B(\nu, T_g) e^{-\tau}\, N_0 R_0{}^2 r^{-2} \pi a^2 Q_{abs}\, ds \quad (4)$$

Where, N_0 is the number density of the grains at R_0 from the source. The product $N_0R_0^2$ is calculated by integrating the N(r) over the volume of the shell, then multiplying by the mass of one grain to find the total mass of grains.

The solution of equation (4) can be simplified by defining a general point
P (θ, θ_1) (Fig. 9). From the figure we can express ds in term of θ and θ_1 as

$$ds = R_{out} \frac{sin\theta_1}{sin^2\,\theta} d\theta \quad (5)$$

Substituting (5) in (4) we get:

$$I_\nu(s) = \int_0^s B(\nu, T_g) e^{-\tau}\, N_0 R_0^2 r^{-2} \pi a^2 Q_{abs}\, R_{out} \frac{sin\theta_1}{sin^2\,\theta} d\theta \quad (6)$$

The corresponding flux is simply the integration of $I_\nu(s)$ over the solid angle Ω, subtended by the region:

$$f_\nu = \int I_\nu cos\theta_1 d\Omega = \frac{\int I_\nu cos\theta_1 2\pi R^2_{out} sin\theta_1}{D^2} d\theta_1 \quad (7)$$

From equations (6) and (7), then

$$f_\nu = \int_{a_1}^{a_2} \int_{b_1}^{b_2} \frac{2\pi^2 N_0 R_0^2}{D^2}\, a^2 V_{exp}\, t\, Q_{abs}\, B(\nu, T_g) e^{-\tau} cos\theta_1 d\theta d\theta_1 \quad (8)$$

Here $R_{out} = V_{exp}\, t$, since the shell grows with time. D is the distance to the nova.

In our model equation (8) is used to calculate the IR flux from the ring and blobs with the relevant limits of integrations.

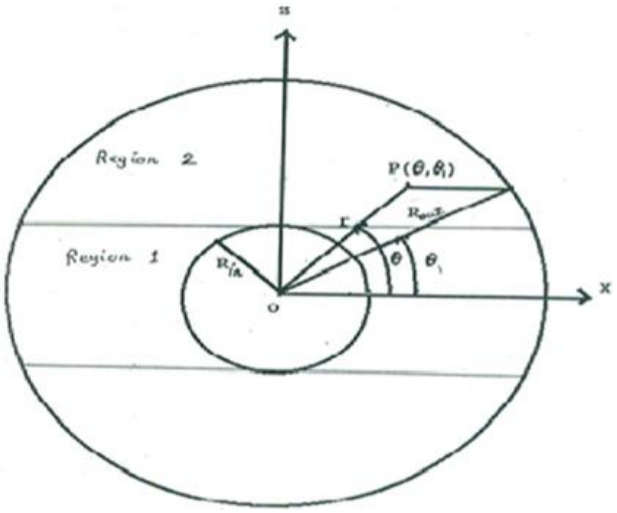

Figure 9: Sketch to illustrate the derivation of the IR equations assuming a general point P(θ, θ1) for spherical shell

4.2 Parameters of Equation (8)

- **The absorption efficiency Q_{abs}**

The equations derived by Mie (1908) are used to find Q_{abs} of the grain [20].The quantity Q_{abs} required for the calculation is given by $Q_{abs} = Q_{ext} - Q_{sca} \rightarrow Q_{abs} = Q_{ext}$ for spherical optically thin shell which is our case.

- **Grain Condensation**

$L_{bol} = 4.0x10^{39}\dot{m}_v$, $V_{exp} = 2.96 \quad 10^{13}\, \dot{m}_v^{.45}\ cm\ day^{-1}$
Where L_{bol} is the bolometric luminosity, measured in erg/s V_{exp} is the expansion velocity. $\dot{m}_v$ is the rate of decline from maximum of the nova in mag. day^{-1} [2].In our calculation $\dot{m}_v$ is taken to be 0.05 mag/day and this correspond to a moderately fast dust forming nova. We choose suitable values for the condensation temperature. T_c, within the range 1200 – 2000 k (e.g. for graphite 2000 k and for silicates 1300 k). The calculated condensation time for graphite & silicate for our model are 32day and 81day respectively.

- **Grain Temperature T_g**

$$T_g = \left[\frac{L < Q_{abs}(a,T_*) >}{16\,\pi\, r^2\, \sigma < Q_{abs}(a,T_g) >}\right]^{\frac{1}{4}} \quad (16)$$

Where for graphite the Planck mean of the absorption efficiencies is approximated by $< Q_{abs}(a,T) >= 3.22\, T^{1.65}$ and that for silicate is taken from [12], $T_* = 10^4 kT$ in the calculations.

- **Optical depth (τ)**

The optical depth τ of equation (8) can be expressed as:

$$\tau = \pi\, a^2 Q_{abs}\, N_0\, R_0^2 \frac{\theta - \theta_1}{V_{exp}\, t\, sin\,\theta_1} \quad (17)$$

5. Results and Discussions

Figures 10, 11, 12 show the IR emission from the model as a function of time at three IR wavelengths (2.2, 3.5, and 10 μm). The behavior of the two maximum of these figures can be ascribed to the different condensation time of graphite grains and silicate grains. Graphite starts condensation first at high temperature around 2000k, while silicate starts

condensation later at around 1300k. a black body at temperature around 2000k emits mainly in the near IR band (λ=2.2µm), while a black body at temperature around 1300 k emits in the far IR band (λ=10µm).

Generally, the result of the IR temporal development calculations in blob-ring Model shows IR light curves of certain distinctive feature, depending on the choice of the infrared band. However three types of curves are distinguished as follows:

a) IR light curve at λ=2.2µm with clear early maximum (solid curve of Fig. 13). This maximum coincides with the maximum optical depth of graphite grains mainly due to graphite emission (solid curve Fig.10).
b) IR light curve at λ=3.5 µm with two maximum (dashed curve of Fig. 13); early maximum and late maximum. The late maximum occurs roughly around the time of maximum optical depth for silicate grains (dashed curve of Fig. 11).
c) IR light curve at λ= 10µm with only one late maximum (dotted curves of Fig.13) being shifted further to later times from the position of silicate maximum optical depth (dashed curve of Fig. 12).

6. Comparison with Observations

The temporal IR flux development shown by the model blob-ring calculations at λ=3.5µm is generally comparable to the IR light curve of nova Cen 1986 (produces graphite and silicate dust) observed by Whitelock (1987) [19] at λ=3.5µm. This similarity can easily be noticed between (Fig. 14, calculations) and (Fig. 15, observations). Both curves of these figures seems to have two maximum separated by a period of time. In the model the length of this period of time depend on the condensation time of the dust material in the two regions. This lead us to conclude that, the second maximum of Nova Cen 1986 was due to silicate dust. This conclusion is supported by observation of Nova V1494 [9].

The model might be improved by using the exact parameters (e.g speed class expansion velocity, density etc….; if known) of one specific nova and then changing one input parameter e.g. grain size to get a fit with the observations.

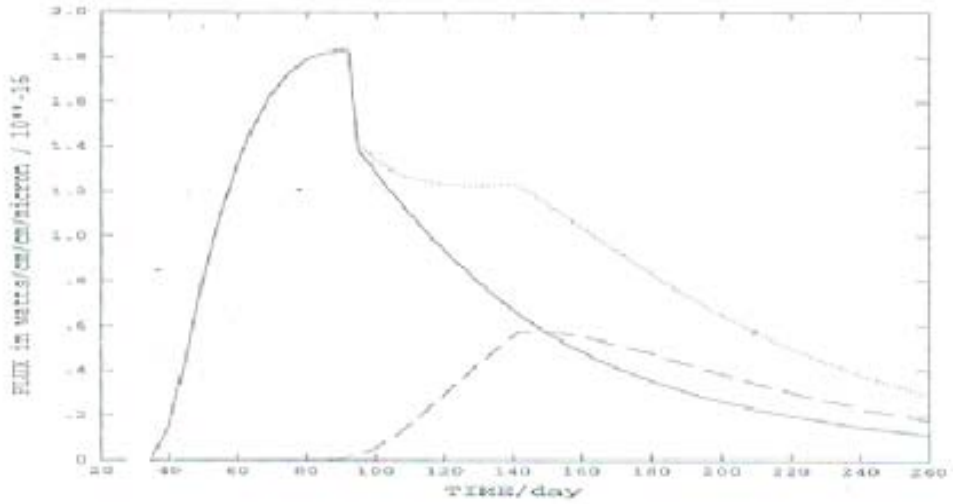

Figure 10: Plot of temporal calculated IR Flux at λ= 2.2 µm. The curves are: solid is emission from the blobs (carbon), dashed is emission from the ring (silicate) and dotted is the result of adding the two together. The speed class is 0.05 mag/ day

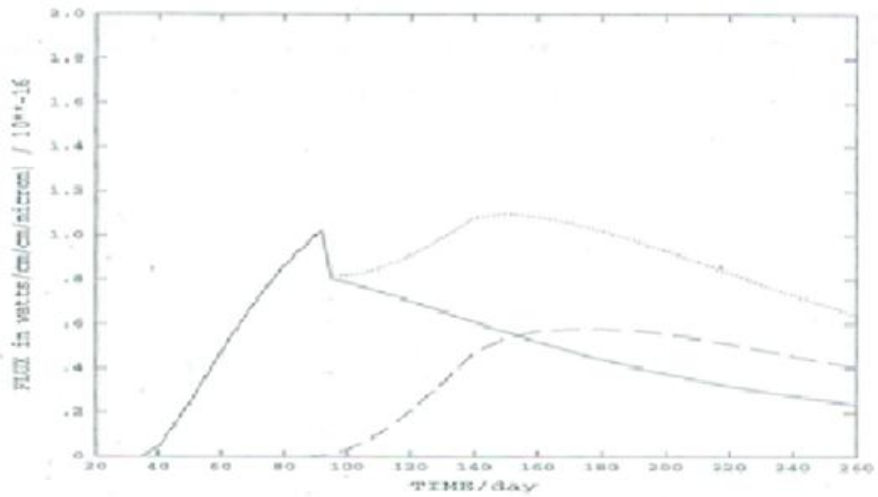

Figure 11: Plot of temporal calculated IR Flux at **λ** = 3.5 µm. The curves are: solid is emission from the blobs (carbon), dashed is emission from the ring (silicate) and dotted is the result of adding the two together. The speed class is 0.05 mag/ day.

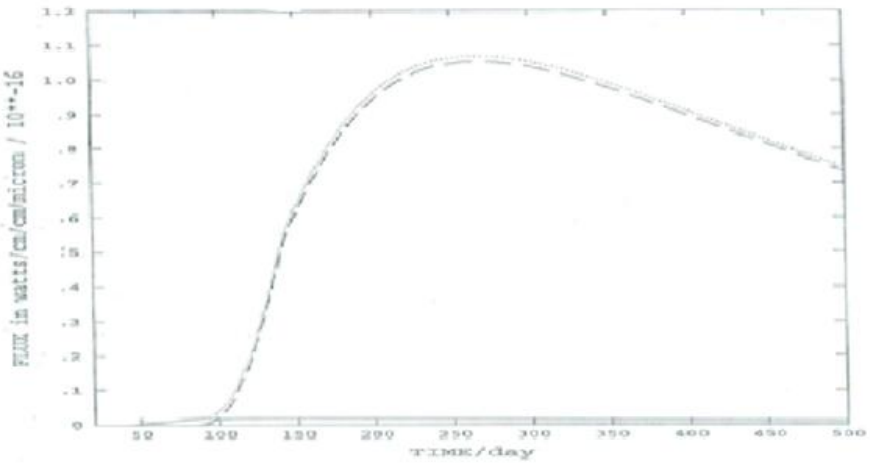

Figure 12: Plot of temporal calculated IR Flux at **λ** = 10 μm. The curves are: solid is emission from the blobs (carbon), dashed is emission from the ring (silicate) and dotted is the result of adding the two together. The speed class is 0.05 mag/ day

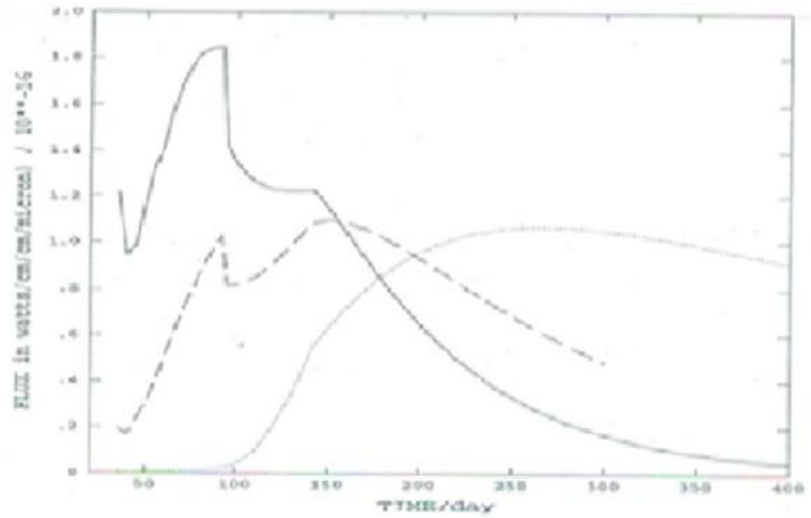

Figure 13: Three temporal calculated IR Fluxes including emission from the star at three wavelengths **λ**= 2.2 μm (solid), **λ**= 3.5 μm (dashed), and **λ**= 10 μm (dotted).

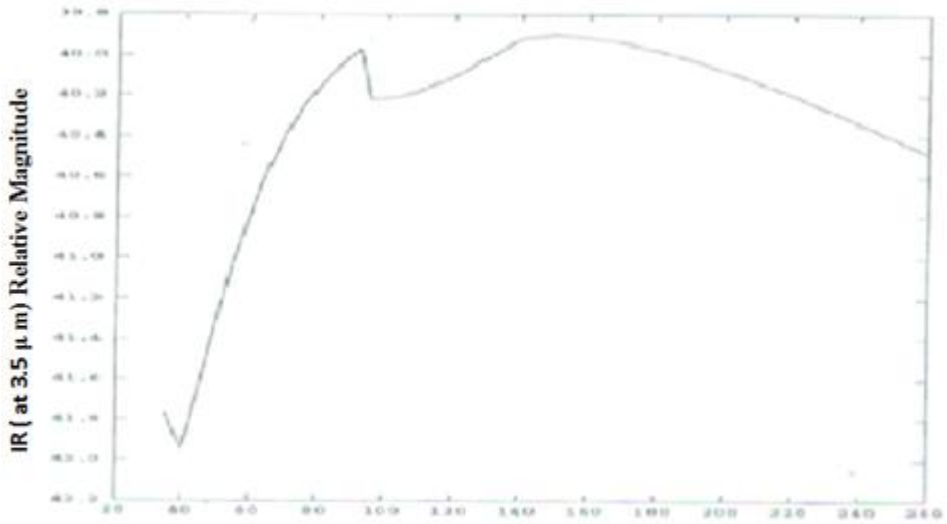

Figure 14: The model temporal calculated IR emission, relative magnitudes at **λ** =3.5 μm.

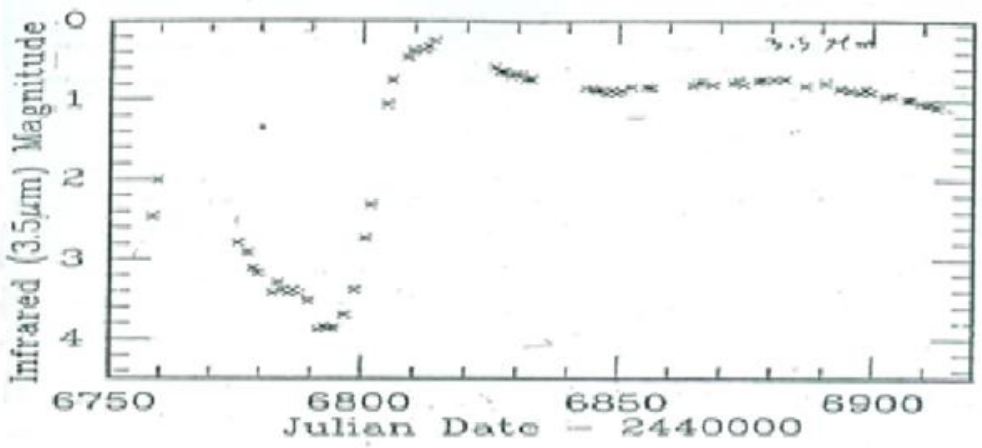

Figure 15: Infrared Light Curve of Cen 1980 at **λ**= 3.5 μm. from Whitelock (1987).

7. Conclusions

According to the model calculations, the behavior of the emitted IR flux can be categorized by three distinctive curves at three infrared wavelengths (near infrared at λ=2.2μm, moderate infrared at λ=3.5μm and far infrared at λ=10μm) (Fig. 10). At near infrared, the IR flux from the blobs is dominating the behavior of the total emitted IR flux. That is the general time behavior of the total IR flux (dotted curve of Fig. 10) is slightly affected by IR flux emission from the ring (solid curve of Fig. 10). And at moderate infrared, the contribution from both graphite in the blobs and silicate in the ring is noticeable (two maxima) in the total flux (Fig. 11). While at far infrared, silicate is the dominant contributor to the total emitted IR flux (Fig. 12).

According to the results of the model, we believe that the blob-ring geometry shell proposed, with dust forming in two different regions (graphite in the blob and silicate in the ring) explains the time and wavelength dependence of the IR emission of some novae.

References

[1] Ashish Raj, Ashok N.M., Banerjee D.P.K. (2013), MNRAS.
[2] Bode, M.F., Evans A., (1982) Visas in Astronomy, V.26, 369-416.
[3] Bode, M.F., Evans A. Whittet, D.C.B., Aitken, D.K., Roche, P.F. and Whitemore, B., (1984) M.N.R.A.S., 207, 897-907.
[4] Chesneau O., Banerjee D.P.K., 2012, Bull.Astro.Soc. India.
[5] Duerbeck, H.W., (1987) ESO Messenger, 50, 8.
[6] Evans, A., (1993) Dusty Universe, Ellis Horwood.
[7] Evans, A., Tyne, V. H., Geballe, T.R., Rawling, T.M., and Eyres, S.P., (2005) Mon. Not. R. Astron. Soc. 360, 1483-1492.
[8] Gehrz, R.D., (1990) In Physics of Classical Movae, IAU Colloquium 122, p.138, eds. Cassetella, a. and Viotti, R., Springer –Velag.
[9] Kamath U.S et al.(2005), MNRAS, 361 (4): 1165-1172.
[10] Harman, D., & O'Brien, T.J., (2003), MNRAS, 344, 1219.
[11] Hutching.J.B., Fisher, W.A., (1972) M.N.R.A.S., 158, 177-198.
[12] Mayse, A.J., (1983), The Circumstellar Dust Distribution Around Variable Stars, Ph.D. Thesis, Keele University, England.
[13] Mclaughlin, D.B., (1960) in Stellar Atmosphere, eds. J.L. Greentein, Chicago; University of Chicago Press.
[14] Mattei, J., (1984) AAVSO Observations, Private communications.
[15] Mustel, E.R., and Boyarchuk, A. A., (1970), Astrophys. Space Sci., 6, 183
[16] Thureau N.D. et al., MNRAS, (2009), 398 (3): 1309 – 1316.
[17] Sato, S., Kawara, K., Kobayashi, Y., et al., (1978), Publ. Astro. Soc.Japan, 30, 419.
[18] Slavin, A, J., O'brien, T.J. and Dunlop, J.S., (1994) M.N.R.A.S., 266, 155-159.
[19] Whitelock, P., (1987) MNASSA, Vol.46, 72.
[20] Wickramasinghe, N.C., (1967), Interstellar Grains (London chapman and Hall).